MINERALOGICAL JOURNAL, VOL. 4, NO. 2, PP. 131-146, AUG., 1963

X-RAY STUDY OF LOW TRIDYMITE (2)

STRUCTURE OF LOW TRIDYMITE, TYPE M

MITSUO SATO

Geological and Mineralogical Institute, Faculty of Science
Tokyo University of Education

ABSTRACT

Lattice constants and space group of low tridymite of type M determined here are: orthorhombic; $a=9.940$A, $b=17.21$A, $c=40.92$A; space group $C222_1$. The long period in the c-direction is caused by minor transverse displacements of constituent atoms along (0 0 1), which simultaneously form the double period in the a-direction, both associated with the phase transition of tridymite.

Introduction

Some interesting facts concerning the structure of low tridymite have been reported, though any conclusive interpretation has not been drawn on the nature of its superstructure (Gibbs, 1927; Buerger & Lukesh, 1942; Flörke, 1955; Fleming & Lynton, 1960). Recently the existence of two types named tridymite M and tridymite S was pointed out by Hill and Roy (1958). In the previous paper, the writer showed that both of them have essentially the same structure as of high tridymite at about 500°C and the difference between them should be attributed to the difference in their structural distortion at high-low transition. The present paper is concerned chiefly with the structure of low tridymite of type M.

1) *Determination of lattice constants and space group*

1-1 *Powder reflections*

Typical X-ray powder data of type M were shown in the previous paper. They show a characteristic strong reflection of 3.25A associ-

ated with a number of weak super-reflections but no doublet. In order to obtain the space lattice and lattice constants of tridymite M, indices of powder reflections were assigned with the aid of reciprocal lattice (Azaroff & Buerger 1958). At first 18 comparatively strong reflections were chosen. The results are shown in Table 1. Indices were then successively assigned to the remaining weak reflections basing on a hexagonal cell of a=9.940A and c=4.092A. The results are listed in Table 2. The appearance of a number of reflections corresponding to ($h\,k\cdot n/10$) indices suggests a hexagonal supper-structure of a=9.940A and c=40.92A.

Table 1. Indexing of 18 chosen reflections and determination of space lattice.

2θ (Cu$K\alpha$)	d(A)	$Q_{obs.}$	$Q_{cal.}$	Δ	$h\ k\ l$
20.60	4.311	0.0538	0.0540	2	2 0 · 0
21.70	4.095	0.0596	0.0597	1	0 0 · 2
23.33	3.813	0.0688	0.0689	1	2 0 · 1
27.48	3.246	0.0949	0.0944	−5	2 1 · 0
28.14	3.171	0.0995	0.1002	7	1 1 · 2
30.11	2.968	0.1135	0.1137	2	2 0 · 2
33.64	2.664	0.1409			
35.28	2.544	0.1545	0.1542	−3	2 1 · 2
36.14	2.485	0.1619	0.1619	0	2 2 · 0
37.73	2.384	0.1759	0.1574	−5	3 1 0
39.09	2.304	0.1884	0.1883	−1	2 0 · 3
43.49	2.081	0.2309	0.2307	−2	4 0 · 1
44.26	2.046	0.2389	0.2389	0	0 0 · 4
45.95	1.975	0.2564	0.2563	−1	3 2 · 0
54.29	1.690	0.3501	0.3502	1	4 0 · 3
59.85	1.545	0.4189	0.4182	−7	5 1 · 0
60.53	1.530	0.4272	0.4272	0	2 0 · 5
66.98	1.397	0.5124	0.5121	−3	4 2 · 3

a^*=0.01012 a=9.940A
c^*=0.01493 c=8.184A
symmetry; hexagonal

Table 2. Indexing of all reflections of tridymite M

2θ	d(A)	$Q_{obs.}$	$h\ k \cdot l$ $\lvert\Delta\rvert \leqq 7$
20.06	4.311	0.0538	2 0 · 0
20.86	4.258	0.0551	1 1 1/2(5/10), 2 0 · 1/8
21.70	4.095	0.0596	0 0 · 2/2(10/10)
23.33	3.813	0.0688	2 0 · 1/2(5/10)
24.35	3.655	0.0744	1 1 · 3/4
25.70	3.466	0.0832	2 0 · 7/10
27.48	3.246	0.0949	2 1 0
27.80	3.209	0.0971	2 1 · 1/5(2/10)
28.14	3.171	0.0995	1 1 2/2(10/10)
28.55	3.126	0.1023	2 1 3/8, 2 0 · 9/10
28.75	3.105	0.1037	2 1 · 2/5(4/10)
29.22	3.056	0.1071	1 0 · 5/4
29.55	3.023	0.1094	2 1 · 1/2(5/10)
30.11	2.968	0.1135	2 0 · 2/2(10/10)
31.48	2.842	0.1238	3 0 · 1/5(2/10), 2 1 7/10
31.79	2.815	0.1262	1 0 · 11/8, 1 1 12/10, 2 0 · 11/10
32.21	2.779	0.1295	2 0 · 9/8, 3 0 · 3/8
32.61	2.746	0.1327	2 1 · 4/5(8/10)
33.64	2.664	0.1409	1 1 13/10
34.51	2.599	0.1480	1 0 · 3/2(15/10)
35.28	2.544	0.1545	2 1 · 2/2(10/10)
36.14	2.485	0.1619	2 2 · 0
36.78	2.444	0.1676	2 2 · 3/10
37.23	2.415	0.1715	2 0 · 13/8, 2 2 · 4/10, 2 0 · 14/10
37.73	2.384	0.1759	3 1 · 0
38.41	2.344	0.1820	3 1 · 2/6
39.09	2.304	0.1884	2 0 · 3/2(15/10)
40.34	2.236	0.2002	3 1 · 3/8, 2 2 · 3/5(6/10)
41.02	2.200	0.2066	1 1 · 10/6, 1 0 · 18/10, 2 0 · 16/10
42.27	2.138	0.2188	4 0 · 1/4, 4 0 · 1/5(2/10)
42.57	2.124	0.2219	3 0 · 13/10, 2 2 · 2/2(10/10)
43.49	2.081	0.2309	4 0 · 1/2(5/10)
44.26	2.046	0.2389	0 0 · 4/2(20/10)
45.01	2.014	0.2465	2 1 · 8/5(16/10)
45.95	1.975	0.2564	3 2 · 0

Table 2 (cont.)

2θ	d(A)	$Q_{obs.}$	$h\ k \cdot l$ $\quad\quad$ $\lvert\Delta\rvert \leqq 7$
46.41	1.956	0.2614	4 0 · 7/8, 3 2 · 3/10, 2 2 · 13/10
46.91	1.937	0.2665	2 1 7/10
47.83	1.902	0.2764	1 0 · 21/10, 3 1 13/10
48.61	1.873	0.2851	4 1 1/6, 3 2 · 7/10
49.36	1.846	0.2935	2 0 · 4/2(20/10), 3 0 · 17/10
49.81	1.831	0.2986	4 1 1/2(5/10)
50.16	1.819	0.3026	1 0 · 11/5(22/10), 4 0 · 6/5(12/10)
51.36	1.779	0.3160	0 0 · 23/10, 3 2 · 2/2(10/10)
51.83	1.764	0.3214	3 0 · 11/6, 4 1 · 4/5(8/10)
52.43	1.745	0.3284	3 1 · 8/5(16/10), 3 2 · 11/10
52.83	1.733	0.3330	2 1 · 4/2(20/10), 4 0 · 7/5(14/10)
53.68	1.707	0.3432	1 1 · 9/4, 4 1 · 2/2(10/10)
54.29	1.690	0.3501	4 0 · 3/2(15/10)
54.82	1.675	0.3569	1 0 · 12/5(24/10), 3 2 · 13/10
56.72	1.623	0.3796	4 2 · 1/6, 3 3 · 1/2(5/10)
57.02	1.615	0.3839	4 2 · 2/6, 1 1 · 24/10, 4 1 13/10
57.77	1.596	0.3926	4 2 1/2(5/10)
58.32	1.582	0.3996	4 1 7/5(14/10), 4 2 3/5(6/10)
59.85	1.545	0.4189	5 1 0
59.89	1.544	0.4195	4 2 · 5/6, 5 1 1/6
60.53	1.530	0.4272	2 0 · 5/2(25/10)
61.30	1.512	9.4374	4 2 · 2/2(10/10), 3 0 · 23/10, 5 0 · 13/10
63.43	1.466	0.4653	3 3 · 13/10, 3 0 · 12/5(24/10), 1 0 · 11/4
64.58	1.443	0.4802	4 0 · 21/10
65.00	1.435	0.4863	6 0 · 1/10
66.03	1.415	0.4994	4 3 · 0, 4 1 19/10, 5 1 7/6
66.73	1.402	0.5095	1 1 · 14/5(28/10), 5 0 · 17/10
66.98	1.397	0.5124	4 2 · 3/2(15/10)
67.13	1.394	0.5146	4 3 · 1/2(5/10), 6 0 · 7/10
67.75	1.383	0.5228	2 0 · 14/5(28/10), 4 1 4/2(20/10)
68.20	1.375	0.5289	4 3 · 7/10, 5 2 · 1/5(2/10)
68.83	1.364	0.5374	4 3 · 4/5(8/10), 3 3 17/10
69.43	1.354	0.5455	2 1 11/4, 3 2 · 11/5(22/10)
69.68	1.349	0.5495	5 2 · 5/8, 3 1 5/2(25/10)
69.98	1.344	0.5536	4 1 17/8, 5 1 · 3/2(15/10)

EXPLANATION OF TABLE 2

In this Table, reflections are indexed based on a hexagonal cell having $a=9.940$A and $c=4.092$A. Thus, $hk\cdot n/10$ indicates a reflection from a unit cell having $a=9.940$A and $c=40.92$A.

Transformation of indices from hexagonal cell $a=9.940$A, $c=4.092$A to orthorhombic cell $a=9.940$A, $b=17.21$A, $c=40.92$A is represented as: $H=h$, $K=h+2k$ and $L=10\cdot n$.

1-2 *Single crystal diffraction*

The small hexagonal platy crystals were collected from the druse of andsite. Oscillation and Weissenberg photographs were then taken with the specimen (Figs. 1 and 2). Among them, strong reflections are due to the subcell corresponding to the high form, and the weak reflections due to the supercell. It is remarkable that most of reflections are intensely diffused along c^* This may be due to the stacking disorder along c^*. Neither super-reflection nor diffuse scattering is noted along c^* among $(00\cdot l)$ reflections. The absence of the doublet and the presence of a strong reflection of (240)*),

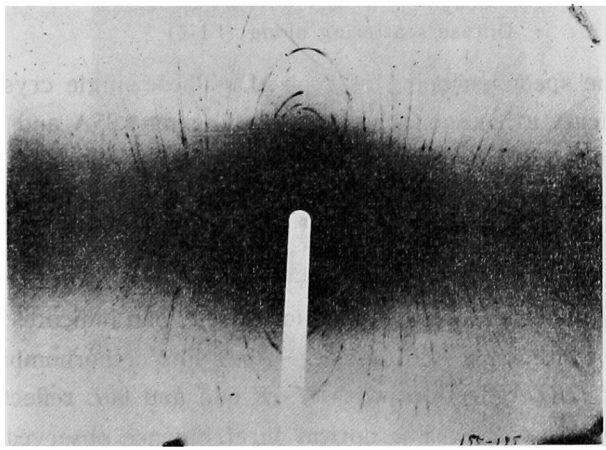

Fig. 1. Oscillation photograph around the c-axis.

*) The characteristic 3.25A reflection of type M is indexed $(1\frac{1}{2}\cdot 0)$ based on the hexagonal subcell or (240) on the orthorhombic supercell.

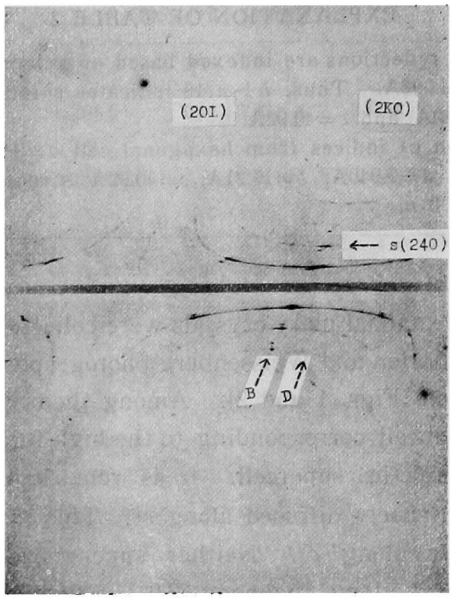

Fig. 2. Weissenberg photograph of (2*KL*) reflections.
s(2 4 0) : super-reflction (2 4 0) peculiar to type M.
B Bragg reflection (2 6 0) {(1 1·0) in the high form index}
D : Diffuse scattering along (1 1·ζ)

indicate the specimen being of type M. These single crystal photograph indicate a hexagonal unit cell having $a \simeq 9.95$A and $c \simeq 41.10$A. These values are in good agreement with those obtained from the powder reflections which were calibrated by an internal standard and are accordingly more accurate.

Since Laue symmetry of $C_{6h}-6/m$ is in conformity with the observation, absence of $00 \cdot l$ reflections with l odd indicates the space group to be either $C_{6h}^2-P6_3/m$ or $C_6^6-P6_3$. For orthorhombic setting, absence of HKL reflections with $H+K$ odd and $00L$ reflections with L odd indicates $C222_1$. The optical birefringence observed along the c axis suggests that it is more appropriate to take the orthorhombic lattice for the analysis to follow. So, the lattice constants and space group are determined as: $a=9.940$A, $b=9.940\times\sqrt{3}\,\text{A}=17.21$A,

c=40.92A, and the space group $C222_1$.

2) *Patterson map*

The intensity of reflections were measured by visual comparison

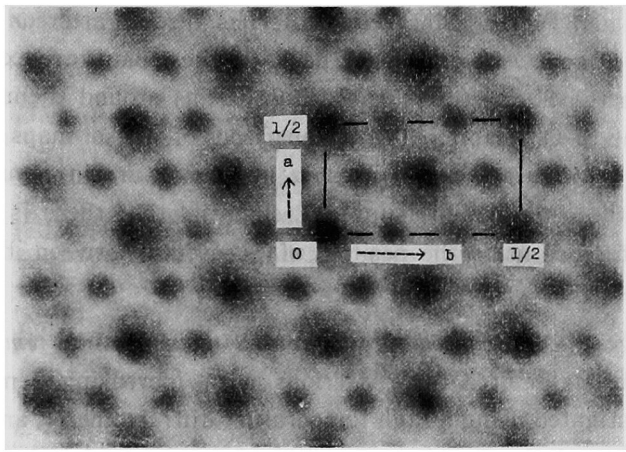

Fig. 3. c-axis Patterson projection.

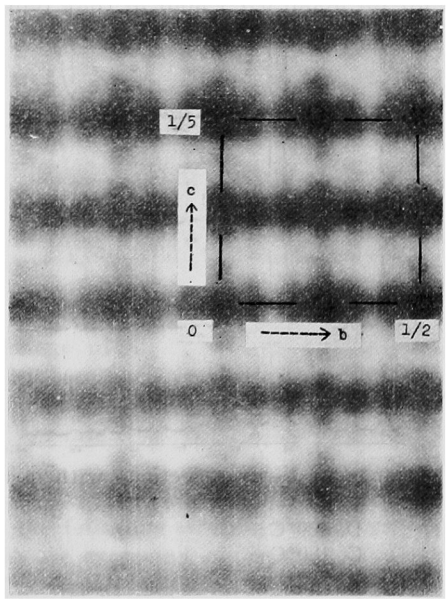

Fig. 4. a-axis Patterson projection.

using the multiple film method in the photographs taken with CuK radiation. Owing to the small linear absorption as well as the small size of the specimen, no correction for absorption was made. Two-dimensional Patterson maps derived from the observed data are shown in Fig. 3 and Fig. 4. Since tridymite has three Patterson vectors; Si-Si, Si-O and O-O, prominent peaks in these maps are expected to be due to the Si-Si vectors and diffused rims around them may be due to the Si-O vectors. The comparison of these maps with the structure of high tridymite, whose a- and c-axes are in common with those of the orthorhombic suprecell, suggests that there is no significant difference as to the position of Si atoms between these two structures.

3) *Change of X-ray powder reflections with increasing temperatures*

The behavior of X-ray reflections with increasing temperatues was investigated using a high temperature diffractometer, and recordings were made by keeping temperature constant after leaving the experimental set-up for about 0.5-1 hour at that temperature (Fig. 5).

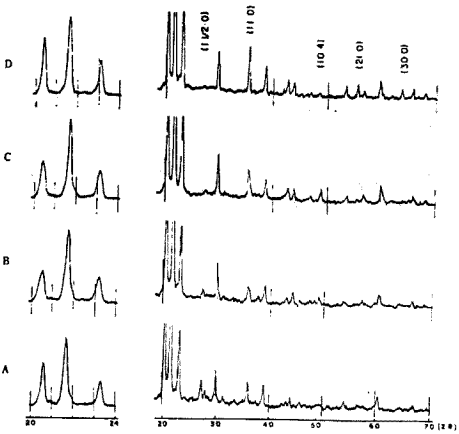

Fig. 5. Change of X-ray reflections with increasing temperatures.
D, 500°C;
C, 180°C;
B, 140°C;
A, room temperature

The patterns should correspond to that of the α form at room temperature, that of the β form at 140°C and those of the γ form at 180°C and 500°C. But as will be seen in the figure, the pattern at 180°C is different a little from that at 500°C, though it has been said that tridymite takes its high form above the second transition point, *i.e.*, about 160°C.

As shown in Fig. 5. reflections subjected to change through the transition are (11·0), (21·0), (30·0), (10·4), ($1\frac{1}{2}$·0)*). The behavior of four reflections was investigated in more detail with the oscillation method. In Fig. 6 is shown the (11·0) reflection, which begins to change its shape at 110°C and increases its intensity continuosly from about 150°C up to 260°C, above which no more change can be confirmed. Fig. 7 is of the (10·4) reflection,

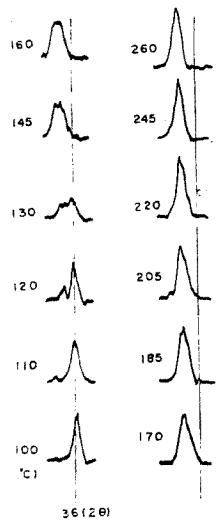

Fig. 6. Change of reflection (11·0) with increasing temperatures (Heating rate, 2.5°C/min.).

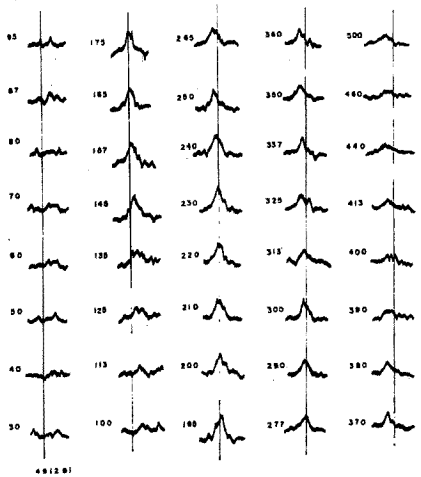

Fig. 7. Change of reflection (10·4) with increasing temperatures.

*) In this and the following sections, the indices based on the hexagonal subcell (high form) are expressed as ($h\,k\cdot l$) and on the orthorhombic supercell as (HKL). The transformation from the hexagonal cell to the orthorhombic is represented as: $H=2h$, $K=2h+4k$ and $L=5l$.

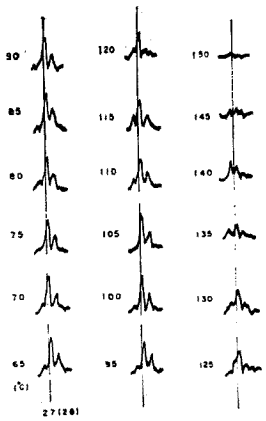

Fig. 8 (a). Change of super-reflections (240) and (242) with increasing temperatures.

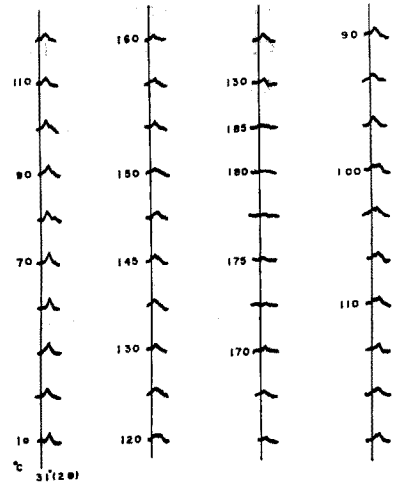

Fig. 8 (b). Change of (332) and (247) super-reflections with increasing and decreasing temperatures.

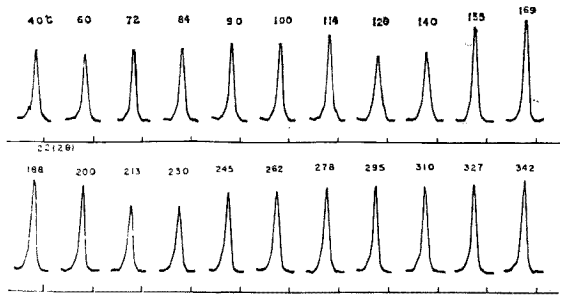

Fig. 9. Change of (0 0·2) reflection with increasing temperatures.

which appears first at 110°C and increases its intensity continuously from about 150°C to 250°C, and above it the reflection becomes broader. Fig. 8(a) shows the characteristic super-reflection (240) associated with (242) peculiar to type M. It decreases its intensity from 110°C and disappears entirely at 150°C. Fig. 8 (b) illustratees super-reflections (332) and (247), which disappears above 170°. The (0 0·2) reflection is also given in Fig. 9.

As the result of these observations, it is obvious that the (1 1·0) and (1 0·4) reflections begin to increase their intensities at about the second transition point, *i. e.*, 150-160°C, while at that point the super-reflections such as (240), (242), (332) and (247) disappear. This suggets that the formation of the long period in the *c*-direction is related to that of the double period in the *a*-direction, both associated with the phase transition.

4) *Structure of low tridymite of type M*

Flörke (1955) explained the supercell of low tridymite being due to the one dimensional polytypism between cristobalite and tridymite layers. This is not always appropriate to account for the observed facts, because 1) There are two kinds of super-reflections. One of them corresponds to the long period in the *c*-direction, and the other to the doubling of period along the *a*-direction. These are both closely related to the phase transition; they simultaneously disappear above the second transition point and reappear after cooling down to room temperature. It is probably impossible for polytypism to occur through this reversible transition because of its small transition entropy (Mosemann & Pitzer 1941). 2) The diffuse scattering along c^* is easy to confirm (Figs. 1 and 2). If it is caused only by the irregular stacking sequence of tridymite and cristobalite layers of the high form, the reflections having $h-k=3n$ (h, k in the high form index) should give Bragg spots along the lines of integral ζ-values, while reflections having $h-k\neq 3n$ give diffuse scattering. Its theoretical treatment are given in Appendix. As seen in Fig. 2, strong reflections due to the hexagonal subcell satisfy this condition. But the appearance of weak diffuse reflections along (1 1·ζ) and (0 3·ζ) with non-integral ζ-values indicates the presence of stacking disorder different from the above.

The alternative way of interpreting the super-structure of low tridymite of type M may be conceived from the facts described in Sections 1, 2 and 3, which are summarized as follows:

(1) No significant difference has been observed as to the positions of Si atoms between high and low tridymites.

(2) The formation of the long period in the c-direction is related to that of the doubling period in the a-direction. These disappear above the second transition point bearing very small transition entropy.

(3) Reflections subjected to change through the phase transition are (a) prismatic reflections, $(1\,1\cdot0)$, $(2\,1\cdot0)$ and $(3\,1\cdot0)$, and (b) superreflection (240) and (c) reflection $(1\,0\cdot4)$.

(4) Neither super-reflection nor diffuse scattering can be observed along c^* among $(00L)$ reflections, while they appear along c^* among (HKL) reflections.

The second and third mentioned above indicate that the long period in the c-direction of low tridymite is caused by minor displacements of constituent atoms along $(0\,0\cdot1)$ normal to c^*, that is, the transverse displacements with reference to the c-direction. These transverse displacements are in conformity with the fact described in (4). The facts in (1) and (3c) also suggest that the displacements may be chiefly of oxygen atoms, because the structure factor of reflection $(1\,0\cdot4)$ is being nearly determined by the contribution of oxygen atoms. The broadness of the $(1\,0\cdot4)$ reflection at high temperature may be due to the vibration of oxygen atoms (Fig. 7). The displacement statistically forms the period of 41A along the c-direction, but the displacements responsible for the doubling of period in the a-direction seems to be random from layer to layer, thus causing the diffuse scattering along c^*.

Appendix

Equations of intensity of X-rays diffracted by a structure derived by stacking disorder between cristobalite and tridymite layers.

The general intensity equation for X-rays diffracted by a one dimensionally disordered crystal was shown (Kakinoki & Komura, 1952 & 1954), for the correlation range of $g=1$, as follows,

$$I=I_e\{N\,\text{spur}\ \boldsymbol{VF}+\sum_{m=1}^{N-1}(N-m)\,\text{spur}\ \boldsymbol{VFQ}^m+\text{conj.}\}.$$

When the thickness of layers are equal,

$$I=I_e\{N\,\text{spur}\ \boldsymbol{VF}+\sum_{m=1}^{N-1}(N-m)\,\text{spur}\ \boldsymbol{VFP}^m\exp(-im\varphi)+\text{conj.}\},$$

Where the symbols mean,

$$\boldsymbol{V}=\begin{bmatrix} V_1^*V_1 & V_1^*V_1 & \cdots\cdots & V_1^*V_R \\ V_2^*V_2 & V_2^*V_2 & \cdots\cdots & V_2^*V_R \\ \vdots & & & \\ V_R^*V_1 & V_R^*V_2 & \cdots\cdots & V_R^*V_R \end{bmatrix}_R, \qquad \boldsymbol{P}=\begin{bmatrix} P_{11} & P_{12} & \cdots & P_{1R} \\ P_{21} & P_{22} & \cdots & P_{2R} \\ \vdots & \vdots & & \vdots \\ P_{R1} & P_{R2} & \cdots & P_{RR} \end{bmatrix}_R,$$

$$\boldsymbol{F}=\begin{bmatrix} W_1 & & & & \\ & W_2 & & & \\ & & \ddots & & \\ & & & \ddots & \\ & & & & W_R \end{bmatrix}_R, \qquad \boldsymbol{\Phi}=\begin{bmatrix} e^{-i\varphi_1} & & & & \\ & e^{-i\varphi_2} & & & \\ & & \ddots & & \\ & & & \ddots & \\ & & & & e^{-i\varphi_R} \end{bmatrix}_R,$$

$$\boldsymbol{Q}=\boldsymbol{\Phi P}$$

V_s : layer form factor of a layer of kind s,

φ_s : phase shift due to the displacement of the layer s along the c direction,

W_s: probability of finding V_s at any q-th position

P_{st} : probability of finding V_t succeeding V_s.

1) Layer form factor of tridymite and cristobalite

The structure of tridymite is looked upon as consisting of two layers A and A' along the c direction. Layer A is stacked upon layer A' by the ratation of 60° around the c-axis. Their layer factors, V_A and V_A', are shown as follows:

$$V_A=\frac{\sin\pi L\xi}{\sin\pi\xi}\frac{\sin\pi My}{\sin\pi y}F_A(hk\zeta)$$

and

$$V_A'=\frac{\sin\pi L\xi}{\sin\pi\xi}\cdot\frac{\sin\pi My}{\sin\pi y}F_A'(hk\zeta),$$

where

$$F_A(hk\zeta)=2f_{si}\varepsilon\cos 2\pi\zeta Z+f_0[\exp \pi i\zeta\cdot\varepsilon+(-1)^h+(-1)^k+(-1)^{h+k}]$$

and

$$F_A'(hk\zeta)=2f_{si}\varepsilon^*\cos 2\pi\zeta Z+f_0[\exp \pi i\cdot\zeta\varepsilon^*+(-1)^h+(-1)^k+(-1)^{h+k}]$$

$$\varepsilon=\exp 2\pi i\frac{h-k}{3}.$$

Cristobalite consists of three layers A, B and C along the [1 1 1] direction. If the hexogonal lattice is taken, layer A can be considered as being put on layers B and C by translations from (0, 0) to (2/3, 1/3) and (1/3, 2/3). Their layer form factors are shown as: V_A, $V_B=V_A\varepsilon^*$, $V_C=V_A\varepsilon$.

2) Layer stacking and the probability of stacking fault

The possible ways of layer stacking for $g=1$ between tridymite and cristobalite layers are as follows:

$$A<\begin{matrix}B\\A'\end{matrix} \qquad A'<\begin{matrix}C'\\A\end{matrix}$$

$$B<\begin{matrix}C\\B',\end{matrix} \qquad B'<\begin{matrix}A'\\B,\end{matrix}$$

$$C<\begin{matrix}A\\C'\end{matrix} \quad \text{and} \quad C'<\begin{matrix}B'\\C.\end{matrix}$$

The P matrix can then shown as

$$\boldsymbol{P}=\begin{array}{c|cccccc} & A & B' & C & A' & B & C' \\ A & 0 & 0 & 0 & 1-\alpha & \alpha & 0 \\ B' & 0 & 0 & 0 & \alpha & 1-\alpha & 0 \\ C & \alpha & 0 & 0 & 0 & 0 & 1-\alpha \\ A' & 1-\alpha & 0 & 0 & 0 & 0 & \alpha \\ B & 0 & 1-\alpha & \alpha & 0 & 0 & 0 \\ C' & 0 & \alpha & 1-\alpha & 0 & 0 & 0 \end{array}$$

3) Intensity equation for $h-k=3n$

When $h-k=3n$, the following relations hold:

$$\varepsilon=\varepsilon^*=1,$$

$$V_A=V_B=V_C=V_A'=V_B'=V_C'=V_0,$$

$$J_m=\text{spur } \boldsymbol{VFP}^m=V_0V_0^*$$

and

$$I(hk\zeta)=I_eV_0V_0^*\frac{\sin^2\pi N\zeta}{\sin^2\pi\zeta}$$

These mean that neither diffuse scattering nor Bragg reflection can be observed along c^* except for reflections along the lines having integral ζ-values.

4) Intensity equation for $h-k=3n\pm1$

In this case, the $\boldsymbol{V}$, $\boldsymbol{F}$ and $\boldsymbol{P}$ matrices are as follows:

$$\boldsymbol{V}=\begin{bmatrix}\boldsymbol{M} & \varepsilon\boldsymbol{M} & \varepsilon^*\boldsymbol{M}\\ \varepsilon^*\boldsymbol{M} & \boldsymbol{M} & \varepsilon\boldsymbol{M}\\ \varepsilon\boldsymbol{M} & \varepsilon^*\boldsymbol{M} & \boldsymbol{M}\end{bmatrix},\quad \boldsymbol{P}=\begin{bmatrix}\boldsymbol{0} & \boldsymbol{UAU} & \boldsymbol{A}\\ \boldsymbol{A} & \boldsymbol{0} & \boldsymbol{UAU}\\ \boldsymbol{UAU} & \boldsymbol{A} & \boldsymbol{0}\end{bmatrix}\text{ and }\boldsymbol{F}=1/6\boldsymbol{E}$$

where

$$\boldsymbol{M}=\begin{bmatrix}V_1^*V_1 & V_1^*V_2\varepsilon^*\\ V_1^*V_2\varepsilon & V_2^*V_2\end{bmatrix},\quad V_1=V_A,\quad V_2=V_A',\quad \boldsymbol{A}=\begin{bmatrix}\alpha & 0\\ 1-\alpha & 0\end{bmatrix}$$

$$\text{and}\quad \boldsymbol{U}=\begin{bmatrix}0 & 1\\ 1 & 0\end{bmatrix}.$$

In the present case, the $\boldsymbol{P}$ matrix cannot be diagonalized, because the minimal polynominal of the $\boldsymbol{P}$ matrix cannot be split into distinct factors, all of the first degree. But in the field of complex numbers, the $\boldsymbol{P}$ matrix can be transformed into the Jordan normal form by a non-singular matrix $\boldsymbol{T}$.

In a matrix $(x\boldsymbol{E}-\boldsymbol{P})$, its elementary divisors are:

$$e_1(x)=e_2(x)=e_3(x)=e_4(x)=e_5(x)=1$$

and

$$e_6(x)=(x-1)\{x+(1-2\alpha)\}\{x^2+\alpha x-(1-2\alpha)\}^2.$$

So,

$$\boldsymbol{TPT}^{-1}=\begin{bmatrix}\boldsymbol{P}_{11} & \boldsymbol{0} & \boldsymbol{0}\\ \boldsymbol{0} & \boldsymbol{P}_{22} & \boldsymbol{0}\\ \boldsymbol{0} & \boldsymbol{0} & \boldsymbol{P}_{33}\end{bmatrix},$$

where

$$\boldsymbol{P}_{11}=\begin{bmatrix} x_1 & 0 \\ 0 & x_2 \end{bmatrix}, \quad \boldsymbol{P}_{22}=\begin{bmatrix} x_3 & 1 \\ 0 & x_3 \end{bmatrix}, \quad \text{and} \quad \boldsymbol{P}_{33}=\begin{bmatrix} x_5 & 1 \\ 0 & x_5 \end{bmatrix},$$

and $\boldsymbol{TPT}^{-1}=\boldsymbol{P}_A$ can be decomposed into $\boldsymbol{P}_S$ and $\boldsymbol{P}_N$, where $\boldsymbol{P}_S$ is a diagonal matrix, $\boldsymbol{P}_N$ a nilpotent matrix and $\boldsymbol{P}_A^m=\boldsymbol{P}_S^m+m\boldsymbol{P}_S^{m-1}\boldsymbol{P}_N$ Now,

$$\begin{aligned}\text{spur } \boldsymbol{VFP}^m &=\text{spur } \boldsymbol{TVFT}^{-1}\boldsymbol{P}_A^m \\ &=\text{spur } \boldsymbol{TVFT}^{-1}(\boldsymbol{P}_S^m+m\boldsymbol{P}_S^{m-1}\boldsymbol{P}_N) \\ &=\sum_{\nu=1}^{5} c_\nu x_\nu^m+m(c_3'x_3^{m-1}+c_5'x_5^{m-1})\end{aligned}$$

and

$$\begin{aligned}I&=I_e\{N\bar{V}^2+\sum_{m=1}^{N-1}(N-m)\,\text{spur } \boldsymbol{VFP}^m \exp(-im\varphi)+\text{conj.}\} \\ &=I_e\{N\bar{V}^2+\sum_{m=1}^{N-1}(N-m)\sum_{\nu=1}^{5} c_\nu x_\nu^m \exp(-im\varphi) \\ &\quad+\sum_{m=1}^{N-1}(N-m)m(c_3'x_3^{m-1}+c_5'x_5^{m-1})\exp(-im\varphi)+\text{conj.}\}\end{aligned}$$

Acknowledgements

The writer is grateful to Prof. T. Sudo for his helpful guidance. He also wishes to express his thanks to Prof. Y. Saito of the Institute for Solid State Physics, University of Tokyo, for his valuable suggestions.

References

Azaroff, L. V. & Buerger, M. J. (1958) : *The powder method in X-ray crystallography.*
Buerger, M. J. & Lukesh, J. (1942) : *Science* **95**, 20.
Flöke, O. W. (1955) : *Ber. Deut. Keram. Gesell.*, **32**, 369.
Gibbs, R. E. (1927) : *Pro. Roy, Soc. London*, **113**, 351.
Hill, V. G. & Roy, R. (1958) : *Trans. Brit. Cream. Soc.*, **57**, 496.
Kakinoki, J. & Komura, Y. (1952) : *Jour. Phys. Soc. Japan*, **7**, 30.
Kakinoki, J. & Komura, Y. (1954) : *Jour. Phys. Soc. Japan*, **9**, 169, 177.
Mosemann, M. A. & Pitzer K. S. (1941) *Jour. Am. Chem. Soc.*, **63**, 2348.

Manuscript received 15 August 1963.